International Journal of Advanced Engineering Research and Science (IJAERS)
Peer-Reviewed Journal
ISSN: 2349-6495(P) | 2456-1908(O)
Vol-12, Issue-6; Jun, 2025
Journal Home Page Available: https://ijaers.com/
Article DOI: https://dx.doi.org/10.22161/ijaers.126.6

Long Wave Analysis using Velocity Potential Equation

Syawaluddin Hutahaean

Ocean Engineering Program, Faculty of Civil and Environmental Engineering-Bandung Institute of Technology (ITB), Bandung 40132, Indonesia.

Received: 19 May 2025,

Receive in revised form: 15 Jun 2025,

Accepted: 21 Jun 2025,

Available online: 26 Jun 2025

Keywords— ***Long Wave, Velocity Potential, Run-up, Inundation***

Abstract— *This research defines long wave as a wave with a large wave period. The analysis is divided into two main components: deep-water analysis and shallow-water analysis. Deep water refers to the initial depth at which wave generation and calculations begin. In the deep-water domain, a formulation for determining wavelength and wave period is developed. In the shallow-water domain, further analyses are conducted to evaluate wave shoaling, breaking, run-up, and flow depth or inundation at the terminal point of the run-up process. The various analytical methods presented in this study are formulated based on the velocity potential approach derived from the solution of the Laplace equation.*

I. INTRODUCTION

Long-periods waves are waves within the range of hundreds to tens of thousands of meters with relatively small amplitudes compared to their lengths. Long-period waves appear in several types, such as tidal waves, tsunamis, and sneaker waves—also referred to as mini tsunamis. Among these, tidal waves with periods of approximately 26.5 hours represent the longest category, with wavelengths extending over thousands of kilometers; however, they fall outside the scope of the present research.

Despite their small amplitudes and extensive wavelengths, such waves often remain undetectable in deep waters. Nevertheless, upon reaching coastal regions, they can suddenly manifest as large, powerful surges capable of inundating areas hundreds of meters or even several kilometers inland. This behavior suggests a substantial energy content inherent in these long waves.

Knowledge on tsunamis is considered comprehensive due to the frequency and destructive impact. Tsunamis are typically generated by geological disturbances beneath the sea, including volcanic eruptions, tectonic plate shifts, subduction processes, and submarine landslides. These events often produce earthquakes, which can serve as precursors to tsunami occurrence. However, it is important to note that not all undersea earthquakes form tsunamis.

Sneaker waves—or mini tsunamis—are another form of long-period waves that possess significant energy and destructive potential in coastal areas. Unlike tsunamis, the mechanisms underlying the formation of sneaker waves remain poorly understood. Nonetheless, due to their capacity for considerable coastal damage, further investigation into these phenomena is necessary.

A key distinction between short and long waves lies in their interaction with the seabed. Short waves are generally unaffected by the seabed in sufficiently deep waters, commonly referred to as “deep water.” For such waves, analytical models typically begin in deep water and incorporate processes such as wave shoaling and breaking to characterize transformations as they approach shallower coastal zones. In contrast, long waves are influenced by the seabed at all depths, effectively rendering all wave motion within shallow water conditions. Consequently, the

characteristics of long waves are significantly affected by the water depth at their point of origin.

Hydrodynamic modeling of tsunamis has been extensively developed, particularly through time series models based on the Boussinesq equations. Notable contributions in this field include works by Kirby et al. (1998), Lynett and Liu (2002), Yamazuki et al. (2011), and Baba et al. (2015), among others.

Some software applications for tsunami analysis are widely available, including:

1. COMCOT
   A numerical model used for tsunami generation, propagation and run-up.
2. Tsunami- N2
   Developed by the National Tsunami Hazard Mitigation Program, widely used for tsunami modeling, hazard assessment and early warning system
3. FLO-2D
   Primarily a flood modeling tool, but also used for tsunami modeling and inundation mapping.
4. GEOWAVE.
   A U.S. Geological Survey (USGS) application for modeling tsunami hazards, integrating data from different sources.
5. TOAST
   A Tsunami Observation and Simulation Terminal, optimized for tsunami early warning applications.
6. TsunAWI
   A modeling software used in the RTSP-Indonesia simulation system, incorporating advanced tsunami source and near-field modeling.

Other applications are mentioned by Suragawa (2021). In the present research, models for long waves, including tsunamis and sneaker waves, were developed based on the velocity potential equation.

The initial stage of model development involved formulating a method for calculating wavelength and wave period using the water depth at the wave generation location or the point of analysis. This reference depth is hereinafter referred to as "deep water depth," although in the context of long waves, it effectively behaves as shallow water due to the influence of the seabed.

Subsequently, a wave transformation analysis method was developed to simulate wave behavior in shallow water conditions. This includes processes such as shoaling, wave breaking, run-up, and the resulting flow depth after the run-up has dissipated.

II. WEIGHTED TAYLOR SERIES AND WEIGHTING COEFFICIENT

Hutahaean (2025) introduced a weighted Taylor series approach, which involves truncating the traditional Taylor series to retain only the first-order terms, with each term modified by a corresponding weighting coefficient.

Weighted Taylor series for a two-variable function $f = f(x,t)$, where x represents the horizontal axis and t is time

$$f(x+\delta x, t+\delta t) = f(x,t) + \gamma_{t,2}\delta t \frac{\mathrm{d}f}{\mathrm{d}t} + \gamma_{x,2}\delta x \frac{\mathrm{d}f}{\mathrm{d}x} \quad \ldots (1)$$

$\gamma_{t,2}$ and $\gamma_{x,2}$ are weighting coefficients with default values $\gamma_{t,2} = 2.0$ and $\gamma_{x,2} = 1.0$. In this research, the equation is used $\gamma_{t,2} = 1.998933$ and $\gamma_{x,2} = 0.998933$.

Weighted Taylor series for function $f = f(x,z,t)$, where x is horizontal axis, and z is the vertical axis and t is time.

$$f(x+\delta x, z+\delta z, t+\delta t) = f(x,z,t) + \gamma_{t,3}\delta t \frac{\mathrm{d}f}{\mathrm{d}t} + \gamma_{x,3}\delta x \frac{\mathrm{d}f}{\mathrm{d}x} + \gamma_{z,3}\delta z \frac{\mathrm{d}f}{\mathrm{d}z} \quad \ldots . (2)$$

$\gamma_{t,3}$, $\gamma_{x,3}$and $\gamma_{z,3}$ are weighting coefficients with default values of, $\gamma_{t,3} = 3.0$, $\gamma_{x,3} = 2.0$ and $\gamma_{z,3} = 2.0$. This research used the coefficient $\gamma_{t,3} = 3.098667$ and $\gamma_{x,3} = \gamma_{z,3} = 2.098667$.

The method used for measuring the weighting coefficients can be seen in Hutahaean (2025).

III. WAVE LENGTH AND WAVE PERIOD ANALYSIS

The analytical method employed in this research is based on the solution of the velocity potential equation derived from the Laplace equation using the method of separation of variables. Following the formulation presented by Dean (1991), the velocity potential is

$$\phi(x,z,t) = G\,(\cos kx + \sin kx)\cosh k(h+z) \sin \sigma t \quad \ldots (3)$$

At a characteristic point where $\cos kx = \sin kx$, the equation becomes,

$$\phi(x,z,t) = 2G \cos kx \cosh k(h+z) \sin \sigma t \quad \ldots (4)$$

In Equations (3) and (4), $\phi(x,z,t)$ is velocity potential, G is wave constants, k is wave number where $k = \frac{2\pi}{L}$, L is wavelength, σ is angular frequency, $\sigma = \frac{2\pi}{T}$, T is wave period, h is water depth.

The relationship between wave amplitude and the wave constant is described through a wave amplitude function developed by Hutahaean (2025), as follows:

a. Hutahaean (2025),

$$A = \frac{2Gk}{\gamma_{t,2}\sigma} \cosh \theta\pi \left(\tanh \theta\pi - \frac{\gamma_{x,2} kA}{2} \right) \quad \ldots . (5)$$

$$A = \frac{\sqrt{2}\, Gk}{\gamma_{t,2}\sigma} \sinh\ \theta\pi \quad \ldots (6)$$

A is wave amplitude and θ is deep water coefficient, where in short wave $\tanh \theta\pi \approx 1.0$. The criteria $\tanh \theta\pi \approx \theta\pi$ is used in this research at an accuracy rate of $\left| \frac{\theta\pi - \tanh \theta\pi}{\tanh \theta\pi} \right| x100\% \leq 5\%$.

In addition to the wave amplitude function, this analysis incorporates two conservation principles: the conservation of energy and the conservation of wave number. For the purposes of this research, the wave number conservation equation, as formulated by Hutahaean (2023a), is utilized in the following form:

$$\frac{dk\left(h + \frac{A}{2}\right)}{dx} = 0 \quad \ldots . (7)$$

where,

$$k\left(h + \frac{A}{2}\right) = \theta\pi \quad \ldots (8)$$

At equation (5), there is a breaking characteristic as follows,

$$\tanh \theta\pi - \frac{\gamma_{x,2} kA}{2} = 0$$

The following relation is obtained,

$$\frac{H_b}{L_b} = \frac{\tanh \theta\pi}{\gamma_{x,2}\pi} \quad \ldots . (9)$$

This indicates that the shoaling analysis based on Equation (5) leads naturally to a wave transformation model that includes the occurrence of breaking as an emergent characteristic.

3.1. Measuring Wavelength in Deep Water.

Assuming that long waves are continuously influenced by the seabed—that is, the wave motion extends to the bottom at all depths—the deep-water wavelength can be approximated using the wave number conservation equation, as expressed in Equation (8). Accordingly, the deep-water wave number is calculated using the following formula.

$$k_0 = \frac{\theta\pi}{h_0(1+\mu)} \quad \ldots (10)$$

In which,

$$\mu = \frac{A_0}{2h_0} \quad \ldots (11)$$

In Equations (10) and (11), the subscript "0" denotes values corresponding to deep water conditions. At the wave generation site—designated as "deep water" for long waves—wave amplitudes are typically very small. This is evident, for example, in the case of sneaker waves, which are generally undetectable in deep water due to their extremely long wavelengths and minimal amplitudes.

Given the relatively small amplitude values used, the resulting parameter μ is a very small quantity and may be considered negligible in the calculation of the deep-water wave number.

3.2. Wave period measurement.

The equation used to measure the wave period was formulated based on Euler's momentum conservation equation 2-D, where the axial system (x,z) consisted of two equations.

At horizontal$-x$ axis direction,

$$\gamma_{t,3} \frac{\partial u}{\partial t} + \frac{\gamma_{x,3}}{2} \frac{\partial uu}{\partial x} = -\frac{1}{\rho} \frac{\partial p}{\partial x} \quad \ldots (12)$$

At vertical-z direction

$$\gamma_{t,3} \frac{\partial w}{\partial t} + \frac{\gamma_{z,3}}{2} \frac{\partial ww}{\partial z} = -\frac{1}{\rho} \frac{\partial p}{\partial z} - g \quad \ldots (13)$$

u and w denote the water particle velocities in the horizontal and vertical directions, respectively, while ρ is water mass density, $\gamma_{t,3}$, $\gamma_{x,3}$ and $\gamma_{z,3}$ are weighting coefficients.

A key modification applied to the governing equations involves the directional dependence of velocity components: the horizontal velocity u component is considered to vary only along the horizontal axis x, while the vertical velocity component w varies only along the vertical axis z. This simplification aligns with the physical assumptions used in formulating the continuity equation and facilitates analytical tractability.

To complete the formulation, it is necessary to derive the pressure equation p. This derivation is based on the velocity potential formulation and incorporates the continuity equation (13). Specifically, the vertical acceleration term $\frac{\partial w}{\partial t}$ is

expressed in terms of horizontal and vertical velocity derivatives using the continuity equation, as formulated by Hutahaean (2012), where it is controlled by continuity equation as follows.

$$\frac{\partial u}{\partial x}+\frac{\partial w}{\partial z}=0 \qquad \ldots(14)$$

This equation is multiplied by dz and integrated to vertical-z axis, from $z=z$, to $z=\eta$, where η is water surface elevation. The outcome of the integration was is differentialized to time-t, where equation $\frac{\partial w}{\partial t}$ is obtained.

$$\frac{\partial w}{\partial t}=\frac{\partial}{\partial t}\int_z^{\eta}\frac{\partial u}{\partial x}dz+\frac{\partial w_\eta}{\partial t}$$

The equation is substituted to (13),

$$\gamma_{t,3}\left(\frac{\partial}{\partial t}\int_z^{\eta}\frac{\partial u}{\partial x}dz+\frac{\partial w_\eta}{\partial t}\right)+\frac{\gamma_{z,3}}{2}\frac{\partial ww}{\partial z} \quad =-\frac{1}{\rho}\frac{\partial p}{\partial z}-g$$

The equation is multiplied by dz and integrated to vertical-z axis, under the threshold of dynamic limit where superficial pressure $p_\eta=0$, and p is obtained. The equation p is differentialized to horizontal-x axis, obtaining

$$\frac{1}{\rho}\frac{\partial p}{\partial x}=\gamma_{t,3}\frac{\partial}{\partial x}\int_z^{\eta}\left(\frac{\partial}{\partial t}\int_z^{\eta}\frac{\partial u}{\partial x}dz\right)dz$$
$$+\frac{\gamma_{z,3}}{2}\frac{\partial}{\partial x}(w_\eta w_\eta-ww)+\left(g+\gamma_{t,3}\frac{\partial w_\eta}{\partial t}\right)\frac{\partial \eta}{\partial x}$$

The equation is substituted to (12),

$$\gamma_{t,3}\frac{\partial u}{\partial t}+\frac{\gamma_{x,3}}{2}\frac{\partial uu}{\partial x}=-\gamma_{t,3}\frac{\partial}{\partial x}\int_z^{\eta}\left(\frac{\partial}{\partial t}\int_z^{\eta}\frac{\partial u}{\partial x}dz\right)dz$$
$$-\frac{\gamma_{z,3}}{2}\frac{\partial}{\partial x}(w_\eta w_\eta-ww)-\left(g+\gamma_{t,3}\frac{\partial w_\eta}{\partial t}\right)\frac{\partial \eta}{\partial x}$$

The final equation was measured at $z=\eta$, obtaining the horizontal particle velocity u at the surface,

$$\gamma_{t,3}\frac{\partial u_\eta}{\partial t}+\frac{\gamma_{x,3}}{2}\frac{\partial u_\eta u_\eta}{\partial x}=-\left(g+\gamma_{t,3}\frac{\partial w_\eta}{\partial t}\right)\frac{\partial \eta}{\partial x}$$

Convective acceleration, represented by the second term on the left-hand side of the equation, is neglected,

$$\gamma_{t,3}\frac{\partial u_\eta}{\partial t}=-\left(g+\gamma_{t,3}\frac{\partial w_\eta}{\partial t}\right)\frac{\partial \eta}{\partial x} \qquad \ldots(15)$$

Using Equation (4),

$$u=-\frac{\partial \phi}{\partial x}=2Gk\sin kx\cosh k(h+z)\sin\sigma t$$

At $z=\eta$,

$$\frac{\partial u_\eta}{\partial t}=2Gk\sigma\sin kx\cosh k(h+\eta)\cos\sigma t$$

The free surface equation is given by,

$$\eta(x,t)=A\cos kx\cos\sigma t$$

$$\frac{\partial \eta}{\partial x}=-kA\sin kx\ \cos\sigma t$$

Substituted to (15),

$$\gamma_{t,3}2Gk\sigma\sin kx\cosh k(h+\eta)\cos\sigma t=$$
$$\left(g+\gamma_{t,3}\frac{\partial w_\eta}{\partial t}\right)kA\sin kx\ \cos\sigma t$$

If $\sin kx\neq 0$ and $\cos\sigma t\neq 0$, common terms on both sides can be eliminated, yielding:

$$\gamma_{t,3}2Gk\sigma\cosh k(h+\eta)=\left(g+\gamma_{t,3}\frac{\partial w_\eta}{\partial t}\right)kA.. \qquad (16)$$

Substituting the wave amplitude A using equation (6), where (Hutahaean (2023)) $\sinh\ \theta\pi$ is $\sinh k(h+\eta)=\sinh k\left(h+\frac{A}{2}\right)$,

$$\gamma_{t,3}2G\sigma\cosh k\left(h+\frac{A}{2}\right)=\left(g+\gamma_{t,3}\frac{\partial w_\eta}{\partial t}\right)$$
$$\frac{\sqrt{2}\,Gk}{\gamma_{t,2}\sigma}\sinh k\left(h+\frac{A}{2}\right)$$
$$\sqrt{2}\gamma_{t,3}\gamma_{t,2}\sigma^2=\left(g+\gamma_{t,3}\frac{\partial w_\eta}{\partial t}\right)\frac{k}{\gamma_{t,2}\sigma}$$
$$\tanh k\left(h+\frac{A}{2}\right) \qquad \ldots.(17)$$

From the velocity potential:

$$w(x,z,t)=-\frac{\partial \phi}{\partial z}=-2Gk\cos kx\sinh k(h+z)$$
$$\sin\sigma t$$

At $z=\eta$

$$\frac{\partial w_\eta}{\partial t}=-2Gk\sigma\cos kx\sinh k(h+\eta)\cos\sigma t$$

Equation (6) is rewritten to express G, and this expression is substituted into the final equation,

$$\frac{\partial w_\eta}{\partial t}=-\sqrt{2}\gamma_{t,2}A\,\sigma^2\cos kx\cos\sigma t$$

This expression is then substituted into Equation (17), evaluated at spatial and temporal characteristic points where $\cos kx=\sin kx$ and $\cos\sigma t=\sin\sigma t$

$$\sqrt{2}\,\gamma_{t,3}\gamma_{t,2}\sigma^2=\left(-\gamma_{t,3}\frac{\sqrt{2}}{2}\gamma_{t,2}A\,\sigma^2+g\right)$$
$$k\tanh\ k(h+\eta)$$

Grouping terms containing σ^2, where at the characteristic point $\eta=\frac{A}{2}$, hence

$$\left(\sqrt{2}+\frac{kA}{\sqrt{2}}\tanh\ k\left(h+\frac{A}{2}\right)\right)\gamma_{t,3}\gamma_{t,2}\sigma^2=$$
$$gk\tanh\ k\left(h+\frac{A}{2}\right)$$

Remembering (8),

$$\left(\sqrt{2}+\frac{kA}{\sqrt{2}}\tanh\theta\pi\right)\gamma_{t,3}\gamma_{t,2}\sigma^2=gk\tanh\ \theta\pi \quad ..(18)$$

This equation is used to calculate the wave frequency σ, from which the wave period can be determined using $T=\frac{2\pi}{\sigma}$. While

this equation applies to both long and short waves, this research specifically focuses on long waves only.

3.3. Example of Wavelength and Wave Period Results. Analysis of θ value.

Table (1) Shows how θ is determined.

θ	δ (%)	L (m)	T (sec)
0.120	4.693	1670.83	161.374
0.121	4.771	1657.03	160.1
0.122	4.849	1643.44	158.848
0.123	4.928	1630.08	157.616
0.124	5.008	1616.94	156.405
0.125	5.088	1604	155.213
0.126	5.169	1591.27	154.041
0.127	5.251	1578.74	152.888
0.128	5.333	1566.41	151.753
0.129	5.416	1554.26	150.636
0.13	5.499	1542.31	149.537

Note: $\delta = \left|\frac{\theta\pi - \tanh\theta\pi}{\tanh\theta\pi}\right| x\ 100\ \%$

Table (1) presents the calculations of wavelength and wave period at water depth $h_0 = 100.0$ m, deep water wave amplitude $A_0 = 0.5$ m for several θ values. As mentioned earlier, this research uses the value of θ where $\delta \approx 5\%$ that corresponds to $\theta = 0.124$. The equation $\theta = 0.124$ is then used.

Table (2) Illustrates the influence of wave amplitude on the wave period and the deep-water wavelength.

A_0 (m)	L (m)	T (sec)
0.1	1613.71	156.226
0.2	1614.52	156.271
0.3	1615.32	156.315
0.4	1616.13	156.36
0.5	1616.94	156.405
0.6	1617.74	156.449
0.7	1618.55	156.494
0.8	1619.36	156.538
0.9	1620.16	156.583
1	1620.97	156.628

In Table (2), the results of calculations for deep-water wavelength and wave period are presented for a water depth of $h_0 = 100.0$ m, $\theta = 0.124$, across several values of deep-water wave amplitude A_0. The results indicate that the influence of wave amplitude is relatively small for both wavelength and wave period. For instance, the difference in wavelength between a wave amplitude of $A_0 = 1.0\,m$ and $A_0 = 0.1\,m$ is:

$$\delta_L = \left|\frac{1620.97 - 1613.71}{1613.71}\right| x100\ \% = 0.45\ \%$$

Similarly, the difference in wave period is,

$$\delta_T = \left|\frac{156.628 - 156.226}{156.226}\right| x100\ \% = 0.257\ \%$$

Subsequently, the influence of deepwater depth h_0 on the deep-water wavelength and wave period is examined. The calculations are performed using $\theta = 0.124$ and $A_0 = 0.5\,m$, which results are shown in Table (3).

As seen in Table (3), wavelength L_0, wave period T and wave celerity C increase with increasing deep-water depth h_0. This indicates that as water depth increases, the increase in wavelength is more significant than the increase in wave period.

Table (3) Influence of deep-water depth h_0 on wavelength and wave period.

h_0 (m)	L_0 (m)	T (sec)	$C = \frac{L}{T}$ (m/sec)
100	1616.94	156.405	10.338
150	2423.39	191.465	12.657
200	3229.84	221.032	14.613
250	4036.29	247.086	16.336
300	4842.74	270.643	17.893
350	5649.19	292.308	19.326
400	6455.65	312.474	20.660
450	7262.1	331.416	21.912
500	8068.55	349.332	23.097

3.4. Comparison with Wavelength from Linear Wave Theory

Previous studies have generally used the wavelength derived from linear wave theory, utilizing the dispersion relation,

$$\sigma^2 = gk \tanh kh \qquad \ldots.(19)$$

For very long wave characteristics, it is commonly assumed that $\tanh kh \approx kh$, obtaining

$$L = T\sqrt{gh} \qquad \ldots.(20)$$

Equation (20) is widely used to calculate the wavelength of long waves. A comparison between the wavelength calculated using Equation (19), denoted L_{19}, and from equation (20) where L_{20}, is presented in Table (4), using a wave period of $T = 300.0\ sec$.

Table (4) The comparison between L_{19} and L_{20}

h (m)	L_{19} (m)	L_{20} (m)	$\frac{L_{20}-L_{19}}{L_{19}} x100$ (%)
100	9389.27	9396.28	0.07
200	13268.5	13288.3	0.15
300	16238.4	16274.8	0.22
400	18736.5	18792.6	0.3
500	20932.4	21010.7	0.37

Although L_{19} is shorter than L_{20} with small difference.

If a weighted Taylor series expansion is applied to the Euler momentum conservation equation, a weighted Bernoulli equation is obtained, in which a weighting coefficient appears. Using this equation, and by following a formulation procedure similar to that of linear wave theory (Dean, 1991), an expression for the free surface elevation that incorporates the weighting coefficient can be derived. This elevation equation is then applied to the weighted Kinematic Free Surface Boundary Condition (KFSBC), while neglecting nonlinear terms—as is typically done in the derivation of the dispersion relation in linear wave theory. This leads to the formulation of a weighted dispersion relation,

$$\gamma_{t,3}\gamma_{t,2}\sigma^2 = gk \tanh kh \qquad \ldots.(21)$$

Further L_{19} is compared to L_{21} from equation (21) and to L_{10} from equation (10), to wave period from equation (18). The comparison is presented in Table (5).

Table (5) The comparison between L_{19} to L_{21} and L_{10}

h (m)	T (sec)	L_{19} (m)	L_{21} (m)	L_{10} (m)
100	192.2	6007.7	2391.1	2002
200	271.7	12012	4780.8	4002
300	332.7	18016.4	7170.5	6002
400	384.2	24020.8	9560.2	8002
500	429.5	30025.1	11949.9	10002

L_{19} is significantly longer than L_{21}, with an average $L_{19} \approx 2.5\ L_{21}$ and $L_{19} \approx 3.0\ L_{10}$. This observation indicates that the weighting coefficient, $\gamma_{t,3}\gamma_{t,2}$, contributes to a substantial reduction in the wavelength calculated in Equation (19). For shorter waves, more accurate wavelength estimations can be made by analyzing natural wave steepness and referring to the critical wave steepness criterion proposed by Toffoli (2000), $\frac{H}{L} = 0.170$. Hutahaean (2023b) stated that based on these criteria, L_{21} and L_{10}. are more closely aligned with the expected values.

Previous studies have reported that tsunami wave models often predict wave arrival times that are several tens of minutes earlier than those observed in nature. This phenomenon has been discussed by Imamura et al. (1990) in their research of the 1960 Chilean tsunami, Rabinovich et al. (2011) regarding the 2004 Sumatra-Andaman earthquake, Fujii and Satake (2013) in the context of the 2010 Chilean earthquake, and Tang et al. (2012) for the 2011 Tohoku event. These researchers have proposed various explanations for the discrepancy in wave propagation speed, including inaccuracies in bathymetric data. However, as demonstrated in the present analysis, the use of linear wave theory tends to overestimate the wavelength. Most existing models employ Equation (20), which is equivalent to Equation (19), as the basis for calculating wavelength. This overestimation of wavelength consequently results in excessively high wave celerity in the models.

A comparison of wave celerity C at deep water between equations (19), (21) and (10) is shown in Table (6, where $C_{19} = \frac{L_{19}}{T}$, $C_{21} = \frac{L_{21}}{T}$ and $C_{19} = \frac{L_{10}}{T}$.

Table (6) The comparison of the wave celerity.

h (m)	T (sec)	C_{19} (m/sec)	C_{21} (m/sec)	C_{10} (m/sec)
100	192.2	31.3	12.4	10.4
200	271.7	44.2	17.6	14.7
300	332.7	54.2	21.6	18
400	384.2	62.5	24.9	20.8
500	429.5	69.9	27.8	23.3

As shown in Table (6), C_{19} with the highest values are $C_{19} = 2.5\ C_{21}$ and $C_{19} = 3.0\ C_{21}$. This significant difference arises from the distinct formulations of the dispersion equation. Upon further examination, the root of this discrepancy lies in the expression of total acceleration within Euler's momentum conservation equation. The linear wave theory is derived from Euler's equation, which utilizes total acceleration formulated through a truncated Taylor series without any weighting coefficients. In contrast, the wave equation derived using a weighted Taylor series yields more accurate results—at least with respect to wavelength estimation. In this research

weighting coefficients were used in wave celerity estimation, through wave period estimation (18).

IV. WAVE TRANSFORMATION ANALYSIS

Wave transformation analysis encompasses the processes of shoaling, breaking, and run-up. The shoaling and breaking equations employed in this research are based on the formulations proposed by Hutahaean (2025).

Given the deep-water input parameters—depth h_0 and A_0 at the starting point,

- T, k_0
- $G_0 = \frac{\gamma_{t,2}\sigma A_0}{\sqrt{2}\,k_0 \sinh\,\theta\pi}$

When a wave propagates from position x at water depth h_x to $x+\delta x$ with water depth $h_{x+\delta x}$, where $h_{x+\delta x} < h_x$, the following changes occur,

a. Change in Wave Number:

$$\frac{dk}{dx} = -\frac{k}{h+\frac{A}{2}+\frac{Gk\lambda}{2}}\frac{dh}{dx} \quad \ldots(22)$$

$$k_{x+\delta x} = k_x + \delta x\frac{dk}{dx}$$

b. Change in wave amplitude

$$\frac{dA}{dx} = \frac{G}{2k}\frac{\mathrm{d}k}{\mathrm{d}x}\lambda \quad \ldots(23)$$

$$\lambda = \frac{1}{\gamma_{t,2}\sigma}\cosh\,\theta\pi\left(\tanh\theta\pi - \frac{\gamma_{x,2}kA}{2}\right) \quad \ldots(24)$$

$$A_{x+\delta x} = A_x + \delta x\frac{dA}{dx}$$

c. Change in wave constant G

$$G_{x+\delta x} = e^{\ln G_x - \frac{1}{2}(\ln k_{x+\delta x} - \ln k_x)} \quad \ldots(25)$$

d. With the updated wave number and wave amplitude, the new wave period is determined using Equation (18).

Equation (18) illustrates that the angular frequency σ is a function of both wave amplitude and wave number. Consequently, any change in wave amplitude and wave number necessitates a recalculation of σ. Therefore, within the shoaling-breaking model, not only the wave amplitude and wave number vary, but the wave period also changes accordingly.

The shoaling-breaking equation is derived by differentiating Equation (5) with respect to the horizontal coordinate x. For simplicity, this research assumes that the influence of the spatial variation of σ is $\frac{d\sigma}{dx}$ negligible in the calculation of the wave amplitude gradient $\frac{dA}{dx}$. Although derivable from Equation (18), $\frac{d\sigma}{dx}$, is not included in the shoaling-breaking computational procedure.

Equation (22) incorporates the run-up phenomenon. Specifically, as long as the condition $\left(h+\frac{A}{2}+\frac{Gk\lambda}{2}\right) > 0$, is satisfied, the calculation proceeds even when the water depth h becomes negative. A negative h value signifies that the seabed elevation is above the still water level, i.e., onshore, thereby indicating the occurrence of run-up.

Based on studies of shortwave profiles, Hutahaean (2024) found that wave profiles in deep water tend to resemble cnoidal waves, whereas in shallow water, they transition into solitary waves—both characterized by profiles entirely above the still water level. From this observation, the concept of effective water depth can be introduced and defined as:

$h_{ef} = h + \alpha H$

In the context of long waves in deep water, a sinusoidal approximation may be valid due to the small wave amplitude relative to the water depth. This assumption introduces minimal error. However, in shallow water, where wave amplitudes are significantly larger, the wave profiles are more accurately described as cnoidal or even solitary waves.

α is a coefficient ranging between $0 < \alpha < 1.0$. This research used $\alpha = 0.6$, considering that $H = 2A$, hence equation (22) becomes,

$$\frac{dk}{dx} = -\frac{k}{h+2\alpha A+\frac{A}{2}+\frac{Gk\lambda}{2}}\frac{dh}{dx} \quad \ldots(26)$$

Where run-up is instantly halted,

$$\left(h+2\alpha A+\frac{A}{2}+\frac{Gk\lambda}{2}\right) \le 0$$

With this formulation, the run-up height increases proportionally, where greater α is followed with greater runup.

The flow velocity within the surge region is calculated using the horizontal particle velocity u,

$$u_{su} = Gk\cosh k(h+2\alpha A) \quad \ldots.(27)$$

As an example of the shoaling, breaking, and run-up analysis, consider waves generated at an initial water depth of $h_0 = 100.0\,m$, where wave amplitude $A_0 = 0.25\,m$, bottom slope

$\frac{dh}{dx} = -0.01$, used $\theta = 0.124$. The results are shown in Fig (1).

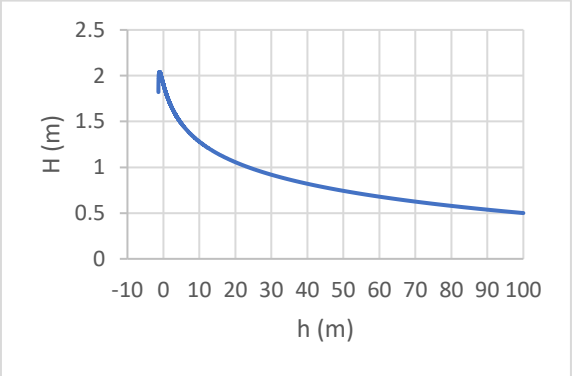

Fig (1) Results of wave transformation analysis.

In Fig. (1), a negative value of water depth h indicates an elevation above the still water level (0.0 m), corresponding to land. According to the results, wave breaking occurs inland at an elevation of +1.086 m, where the water surface elevation reaches +2.040 m. The wave run-up terminates at an elevation of +1.396 m, with the water surface at +1.799 m, transitioning into a surge. If beyond the elevation of +1.396 m the topographic slope decreases or flattens, a landward surge occurs with a flow depth h_{su} = (1.799-1.396) m = 0.403 m, and a flow velocity $u_{su} = 0.950\ m/sec$. The wave run-up and the initiation point of the surge is illustrated as follows:

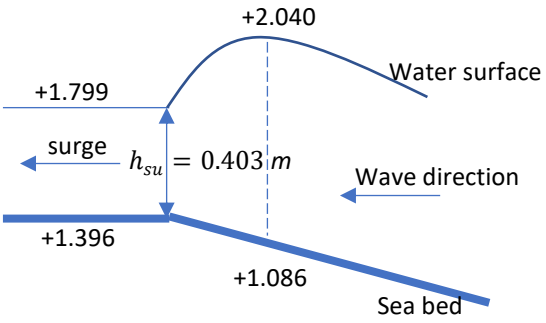

Fig (2). Wave run-up and surge on land

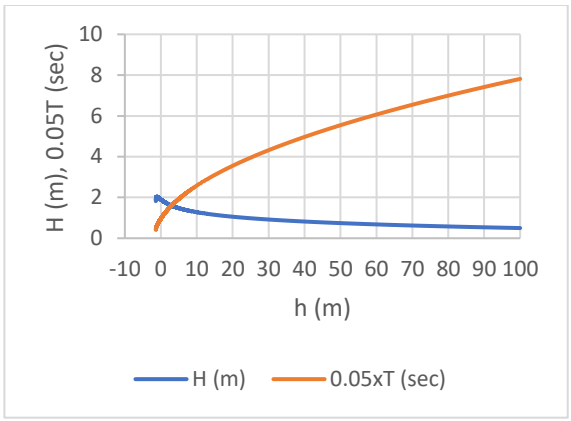

Fig (3). Changes in wave period T.

In the shoaling-breaking process, wave amplitude, wave number and wave period change. Figure 3 illustrates the change in wave period, where the initial deep-water period is $T = 156.293\ sec.$ and decreased to $T = 8.135\ sec.$

As previously discussed, the influence of deep-water wave amplitude on the wavelength and wave period is relatively minor. However, in the following section, it will be demonstrated that the deep-water wave amplitude has a substantial impact on both the breaking wave height and the run-up. Table (7) presents the calculation results for an initial depth of $h_0 = 100.0\ m$, cross various wave amplitudes, with a bottom slope of $\frac{dh}{dx} = -0.01$ and deep-water coefficient $\theta = 0.124$.

Table (7) The effect of deep-water wave amplitude A_0 on the breaking wave height.

A_0 (m)	T_0 (sec)	T_a (sec)	H_{br} (m)	h_{br} (m)
0.1	156.226	5.111	0.926	-0.499
0.2	156.271	7.253	1.685	-0.901
0.3	156.315	8.658	2.384	-1.266
0.4	156.36	9.9	3.042	-1.607
0.5	156.405	10.622	3.673	-1.932
0.6	156.449	11.691	4.28	-2.243
0.7	156.494	12.582	4.869	-2.543
0.8	156.538	13.367	5.442	-2.833
0.9	156.583	13.88	6.001	-3.115
1	156.628	14.509	6.548	-3.391

Note: T_0: deep water wave period

T_a: wave period at the end point, corresponding to the onset of the surge.

The results indicate that the deep-water wave amplitude has a minimal effect on the deep-water wave period. However, its impact on the breaking wave height H_{br} and the run-up is considerable. An increase in wave amplitude of just 0.10 m leads to an average increase in breaker height of approximately 0.6–0.7 m. Similarly, the elevation at which the surge begins $|h_{end}|$ also increases. Flow depth surge h_{su} also increases, as shown in Table (8).

Table (8) Depth h_{su} and surge velocity u_{su}.

A_0 (m)	H_{end} (m)	h_{end} (m)	h_{su} (m)	u_{su} (m/sec)
0.1	0.793	-0.641	0.152	0.69
0.2	1.493	-1.157	0.336	0.858
0.3	2.101	-1.627	0.474	1.068
0.4	2.782	-2.068	0.714	1.215
0.5	3.166	-2.488	0.678	1.481
0.6	3.748	-2.891	0.857	1.551
0.7	4.323	-3.28	1.042	1.653
0.8	5.053	-3.658	1.395	1.761
0.9	5.22	-4.025	1.195	1.944
1	5.686	-4.384	1.302	2.061

H_{end} refers to the wave height—or more precisely, the water surface elevation—at the point where the wave transitions into a surge. Whereas, h_{end} denotes the land surface elevation at this transition point, where the wave transforms into a surge with a corresponding surge flow depth h_{su}. For instance, if $A_0 = 0.50\ m$, the wave transforms into a surge at an elevation of +2.488 m, with a surge flow depth of $h_{su} = 0.678\ m$, with surge velocity $u_{su} = 1.481\ m/sec$.

The, the influence of deep-water depth h_0 on wave height H_{br} is analyzed. Calculations are conducted using a deep-water wave amplitude of $A_0 = 0.25\ m$, bottom slope $\frac{dh}{ex} = -0.01$, at deep water coefficient $\theta = 0.124$. The results are presented in Table (9).

Table (9). Breaking wave height H_{br} at several deep-water depths h_0.

h_0 (m)	T_0 (sec)	H_{br} (m)	h_{br} (m)
100	156.293	2.04	-1.086
150	191.374	2.161	-1.158
200	220.953	2.248	-1.209
250	247.015	2.316	-1.249
300	270.579	2.371	-1.282
350	292.248	2.418	-1.31
400	312.419	2.459	-1.334
450	331.363	2.495	-1.355
500	349.282	2.528	-1.374

As shown in Table (9), an increase in deep-water depth generally results in an increase in the breaking wave height. However, this increase diminishes with greater values of $h_0 = 100\ m$ to $h_0 = 150\ m$, the increase in H_{br} is $0.121\ m$. Meanwhile, from $h_0 = 450\ m$ to $h_0 = 500\ m$, the increase in H_{br} is $0.036\ m$. These results suggest that errors in bathymetry data, particularly at large depths, do not lead to significant inaccuracies in the estimation of breaking wave height.

V. CONCLUSION

The model developed in this research is capable of simulating long-wave behavior in coastal waters, including wave run-up, flow depth, and current velocity at the onset of inundation. As such, it can be effectively utilized to estimate a range of hazards or impacts associated with long waves in coastal and nearshore areas.

Regarding the model's accuracy, further validation is necessary, particularly through comparisons with empirical data and findings from previous field-based studies. In this research, the resulting wavelengths are significantly shorter than those predicted by linear wave theory, with wave celerity reduced to approximately one-third of that given by the linear model. Several prior studies have reported that numerical models employing wavelengths derived from linear wave theory predict tsunami arrival times that are tens of minutes earlier than actual observations. In this respect, the present research is consistent with such findings. When early warning systems are based on linear wave theory, they may predict tsunami arrival times prematurely. Nevertheless, this conservative prediction provides the advantage of allowing earlier emergency preparedness and response.

One limitation of the model is its inability to predict the full extent of inland surge propagation. The model can only determine the location where the wave transitions into a surge. However, a simple estimation can be made: the maximum inland extent of the surge or inundation is likely to correspond to the elevation of the water surface at the point where the surge forms.

REFERENCES

[1] Kirby, J.T., Wei, G., Chen, G.,Kennedy, A.B. Dalrymple, R.A. FUNWAVE 1.0, Fully Nonlinear Bousinesq Wave Model. Documentation and User's Manual, Res.Rep. No. CACR-98-06, Center. for Appl.Coastal Res., Dept.Civil Eng., Univ.of Delaware.

[2] Lynett, P.J., Liu, P/L-F. (2002). Modeling Wave Generation, evolution and interaction, with depth-integrated dispersive wave equations. COULWAVE Code Manual, Cornell University Langand Intermediate Wave Modeling Package (2002).

[3] Yamazuki, Y., Cheung, K.F., Kowalik, Z (2011). Depth Integrated Nonhydrostatic Model With Grid Nesting for Tsunami Generation, Propagation and Run-up. Int.J.Numer. Methods Fluid., 67(2011), pp.2081-2107, 10.1002/fld.2485.

[4] Baba, T., Takahashi, N. Kaneda, Y., Ando, K., Matsuoka, D., Kato,T.(2015). Parallel Implementation of Dispersive Tsunami Wave Modeling with A Nesting Algorithm for The2011 Tohoku Tsunami. Pure Appl.Geophys.,172(2015), pp.3455-3472, 10.1007/s00024-015-1049-2.

[5] Suragawa, D. (2021). Numerical Modeling of Tsunami: Advances and Future Chalenges after the (2011) Tohoku Earthquake and Tsunami. Earth-Science-Reviews. Volume 214, March 2021, 103498.

[6] Hutahaean, S. (2025). New Weighted Taylor Series for Water Wave Energy Loss and Littoral Current Analysis. International Journal of Advance Engineering Research and Science (IJAERS). Vol. 12, Issue 1; Jan, 2025, pp 27-39. Article DOI: https://dx.doi..org/10.22161/ijaers.121.3.

[7] Dean, R.G., Dalrymple, R.A. (1991). Water wave mechanics for engineers and scientists. Advance Series on Ocean Engineering.2. Singapore: World Scientific. ISBN 978-981-02-0420-4. OCLC 22907242.

[8] Hutahaean, S. (2023a). Water Wave Velocity Potential on Sloping Bottom in Water Wave Transformation Modeling. International Journal of Advance Engineering Research and Science (IJAERS). Vol. 10, Issue 10; Oct, 2023, pp 149-157. Article DOI: https://dx.doi..org/10.22161/ijaers.1010.15.

[9] Hutahaean, S. (2012). Pemodelan Gelombang dengan Menggunakan Tekanan Hidrodinamis yang Dirumuskan dari Persamaan Kontinuitas Untuk Fluida Berakselerasi. Jurnal Teknik Sipil ITB.

[10] Toffoli, A., Babanin, A., Onaroto, M. and Wased, T. (2010). Maximum steepness of oceanic waves: Field and laboratory experiments.Geophysical Research Letters. First published 09 March 2010. https://doi.org/10.1029/2009GL.0441771.

[11] Hutahaean, S. (2023b). Method for Determining Weighting Coefficients in Weighted Taylor Series Applied to Water Wave Modeling. International Journal of Advance Engineering Research and Science (IJAERS). Vol. 10, Issue 12; Dec, 2023, pp 105-114. Article DOI: https://dx.doi..org/10.22161/ijaers.1012.11.

[12] Imamura, F., Shuto, N., Goto, C.(1990). Study on Numerical Simulation of the Transoceanic Propagation of Tsunami. Zishin (Ser.2), 43 (1990), pp. 389-402, 10.4294/zisin1948-43.3_389

[13] Rabinovich, A.B., Woodworth, P.L., Titov, V.V. (2011). Deep-sea Observation and Modeling of the 2004 Sumatra Tsunami in Drake Passage.. Geophys.Res.Lett., 38(2011), Article L16604, 10.1029/2011GL0483305.

[14] Fujii, Y., Satake, K. (2013). Slip Distribution and Seismic Moment of the 2010 and 1960 Chilean Earhquakes Inferred from Tsunami Waveforms and Coastal Geodetic data. Pure Appl.Geophys., 170 (203), pp. 1493-1509, 10.1007/s00024-012-0524-2

[15] Tang, L., Titov, V.V., Bernard, E.N., Wei, Y., Chamberlin, C.D., Newman, J.C., Mofjeld, H.O., Arcas, D., Eble, M.C. Moore, C., Uslu, B.,Pells, C., Spillane, M., Wright, L., Gica, E. (2012). Direct Energy Estimation of the 2011 Japan Tsunami Using Deep Ocean Pressure Measurements. J.Geophys.Res. 117(2012), Article C08008, 10-1029/2011J007635.

[16] Hutahaean, S. (2024). Periodic Water Waves: Cnoidal and Solitary Profiles. International Journal of Advance Engineering Research and Science (IJAERS). Vol. 11, Issue 11; Nov, 2024, pp 28-34. Article DOI: https://dx.doi..org/10.22161/ijaers.1111.4.